LETTER **Communicated by Peter J. Thomas**

A General, Noise-Driven Mechanism for the 1/f-Like Behavior of Neural Field Spectra

Mark A. Kramer
mak@bu.edu
Department of Mathematics and Statistics, and Center for Systems Neuroscience, Boston University, Boston, MA 02214, U.S.A.

Catherine J. Chu
cjchu@mgh.harvard.edu
Department of Neurology, Massachusetts General Hospital and Harvard Medical School, Boston, MA 02114, U.S.A.

Consistent observations across recording modalities, experiments, and neural systems find neural field spectra with 1/f-like scaling, eliciting many alternative theories to explain this universal phenomenon. We show that a general dynamical system with stochastic drive and minimal assumptions generates 1/f-like spectra consistent with the range of values observed in vivo without requiring a specific biological mechanism or collective critical behavior.

1 Introduction

Transient oscillations are a prominent feature of macroscopic neural field activity (Buzsaki, 2011) linked to brain function (Buzsaki & Draguhn, 2004) and dysfunction (Gibbs et al., 2002; Uhlhaas & Singer, 2012). Oscillations appear as narrowband increases in the spectrum above an aperiodic background in which the power P decreases proportional to the frequency f raised to an exponent β: $P \propto f^{\beta}$. Characterizing oscillations while accounting for the aperiodic background is important for understanding neural spectra (Donoghue et al., 2020). Sophisticated methods (Donoghue et al., 2020; Wen & Liu, 2016; Wilson et al., 2022) support estimation of the 1/f-like, scale-free (He, 2014) or power-law (Newman, 2005) behavior of neural field spectra. Changes in β, the aperiodic exponent, have been investigated in many domains, including sleep (Bódizs et al., 2021; Freeman & Zhai, 2009; Horváth et al., 2022; Lendner et al., 2020), aging (Cesnaite et al., 2023; Schaworonkow & Voytek, 2021; Voytek et al., 2015), and disease (Lanzone et al., 2022; Numan et al., 2022; Robertson et al., 2019). While many factors have an impact on estimation of the aperiodic exponent (e.g., the frequency range analyzed; (Gerster et al., 2022; Stumpf & Porter, 2012), values of the

Neural Computation **36, 1643–1668** (2024)
https://doi.org/10.1162/neco_a_01682

Table 1: Example Aperiodic Exponents for Human Voltage Spectra Reported in the Literature.

β	Reference	Recording Modality	Frequency	Experimental Condition
−0.08	(Colombo et al., 2019)	Scalp EEG ($n = 5$)	20–40 Hz	Anesthesia (ketamine)
−1.12	(Lanzone et al., 2022)	Scalp EEG ($n = 16$)	1–40 Hz	Eyes closed
−1.3	(Adelhöfer et al., 2021)	Scalp EEG ($n = 74$)	2–40 Hz	Behavioral experiments
−1.44	(Adelhöfer et al., 2021)	Scalp EEG ($n = 74$)	2–40 Hz	Behavioral experiments
−1.48	(Lanzone et al., 2022)	Scalp EEG ($n = 18$)	1–40 Hz	Stroke patients
−1.51	(Robertson et al., 2019)	Scalp EEG ($n = 78$)	4–50 Hz	Resting state
−1.67	(Robertson et al., 2019)	Scalp EEG ($n = 76$)	4–50 Hz	Resting state
−1.84	(Lendner et al., 2020)	Scalp EEG ($n = 9$)	30–45 Hz	Wakefulness
−1.86	(Fransson et al., 2013)	Scalp EEG ($n = 7$)	0.2–30 Hz	Sleep
−1.87	(Lendner et al., 2020)	Scalp EEG ($n = 14$)	30–45 Hz	Resting state
−2.03	(Colombo et al., 2019)	Scalp EEG ($n = 5$)	20–40 Hz	Wakefulness
−2.07	(Fransson et al., 2013)	Scalp EEG ($n = 15$)	0.2–30 Hz	Sleep
−2.32	(Freeman et al., 2000)	Intracranial EEG ($n = 5$)	0.5–150 Hz	Resting state
−2.33	(Bódizs et al., 2021)	Scalp EEG ($n = 175$)	2–48 Hz	NREM sleep
−2.44	(He et al., 2010)	Intracranial EEG ($n = 5$)	1–100 Hz	Wakefulness
−2.48	(Colombo et al., 2019)	Scalp EEG ($n = 5$)	20–40 Hz	Wakefulness
−2.71	(Horváth et al., 2022)	Scalp EEG ($n = 251$)	2–48 Hz	NREM sleep
−2.73	(Bódizs et al., 2021)	Scalp EEG ($n = 175$)	2–48 Hz	NREM sleep
−2.75	(Lendner et al., 2020)	Intracranial EEG ($n = 12$)	30–45 Hz	Wakefulness
−2.87	(He et al., 2010)	Intracranial EEG ($n = 5$)	1–100 Hz	Slow wave sleep
−2.99	(Lendner et al., 2020)	Intracranial EEG ($n = 10$)	30–45 Hz	Wakefulness
−3.1	(Lendner et al., 2020)	Scalp EEG ($n = 9$)	30–45 Hz	Anesthesia
−3.13	(Colombo et al., 2019)	Scalp EEG ($n = 5$)	20–40 Hz	Wakefulness
−3.46	(Lendner et al., 2020)	Scalp EEG ($n = 14$)	30–45 Hz	N3 Sleep
−3.59	(Colombo et al., 2019)	Scalp EEG ($n = 5$)	20–40 Hz	Anesthesia (xenon)
−3.67	(Lendner et al., 2020)	Scalp EEG ($n = 14$)	30–45 Hz	N2 sleep
−3.69	(Lendner et al., 2020)	Intracranial EEG ($n = 10$)	30–45 Hz	N3 sleep
−4	(Miller et al., 2009)	Intracranial EEG ($n = 20$)	80–500 Hz	Behavioral experiments
−4.15	(Lendner et al., 2020)	Intracranial EEG ($n = 10$)	30–45 Hz	REM sleep
−4.34	(Lendner et al., 2020)	Intracranial EEG ($n = 12$)	30–45 Hz	Anesthesia
−4.36	(Colombo et al., 2019)	Scalp EEG ($n = 5$)	20–40 Hz	Anesthesia (propofol)
−4.73	(Lendner et al., 2020)	Scalp EEG ($n = 14$)	30–45 Hz	REM sleep

Notes: The mean value of the aperiodic exponent (β) reported in the reference listed in the Reference column. Additional details include recording modality, number of subjects n, frequency range analyzed, and experimental condition. Considering only studies with minimum frequencies $\geq$20 Hz (shaded rows), the aperiodic exponent has mean −3.1, lower quartile −4, and upper quartile −2.5.

exponent reported at higher frequencies (>20 Hz) typically range between −4 and −2 (see Table 1).

The universal observation of 1/f-like neural field spectra with a restricted range of aperiodic exponents across different recording modalities, experiments, and neural systems suggests a common generative mechanism. However, many complex, specific mechanisms have been identified to generate this phenomenon. These include excitatory/inhibitory balance (Gao et al., 2017), low-pass frequency filtering by dendrites (Buzsáki et al.,

2012) or the extracellular medium (Bédard et al., 2006), nonideal resistive components in the cell membrane (Bédard & Destexhe, 2008), stochastic firing of neurons convolved with an exponential relaxation process (Bédard et al., 2006; Miller et al., 2009; Milstein et al., 2009), stochastic synaptic conductances (Rudolph et al., 2005), stochastically driven damped oscillators with different relaxation rates (Evertz et al., 2022), local homogeneous connectivity (Jirsa, 2009), combinations of many transient oscillations at different frequencies and amplitudes (He et al., 2010), or network mechanisms linking slower rhythms to broad neuronal recruitment and therefore larger amplitude field potentials (Buzsáki et al., 2012). Theoretically, scale-free phenomena, with 1/f-like behavior, have been linked to fractal properties (Pritchard, 1992), critical transitions (Newman, 2005; O'Byrne & Jerbi, 2022), and self-organized criticality (Bak et al., 1987; Cocchi et al., 2017). How these proposed biological and mathematical mechanisms contribute, separately or combined, to the range of aperiodic exponents observed across diverse neural field spectra remains unclear.

Here we demonstrate how, in general, a dynamical system with stochastic drive generates 1/f-like behavior at higher frequencies in neural field spectra. We show that two noise terms, representing correlated and uncorrelated noise inputs, produce the range of aperiodic exponents observed in vivo. We illustrate these general results in nonlinear models of neural and nonneural activity to demonstrate the ambiguity in determining the specific mechanisms given only the observed 1/f-like behavior in the spectrum. While more complex underlying mechanisms may exist, we instead illustrate how the range of aperiodic exponents observed in vivo occurs in general for dynamical systems with stochastic drive, without requiring a specific biological mechanism or tuning to collective critical behavior.

2 Results

As a general model of neural activity, we consider the n-dimensional dynamical system,

$$\frac{dX_k}{dt} = f_k(X_1, X_2, \ldots, X_n) + \sum_{j=1}^{m} B_{kj}\epsilon_{X,j}, \tag{2.1}$$

where, for each $k = \{1, 2, \ldots, n\}$, X_k is a one-dimensional variable, f_k is a nonlinear function, B_{kj} is a constant, and $\epsilon_{X,j}$ is an independent gaussian white noise source with mean zero and variance $\sigma^2_{X,j}$. We assume the variable X_1 (i.e., $k = 1$) is an observable quantity (e.g., the voltage recorded in the EEG or LFP) and all other variables ($X_2, X_3, \ldots, X_n$) represent $n - 1$ unobserved or latent variables affecting the observable dynamics. The unspecified model, equation 2.1, is general and therefore consistent with diverse

models of neural activity. To derive the main result from this general model requires no specific biophysical mechanism. In what follows, we illustrate these general results by making specific model choices for the variables (X_k) and functions (f_k).

We assume an equilibrium exists in the noise-free model so that $\left(\frac{dX_1}{dt}, \frac{dX_2}{dt}, \ldots, \frac{dX_n}{dt}\right) = (0, 0, \ldots, 0)$ at $(X_1, X_2, \ldots, X_n) \equiv \vec{X}^0$. Near this equilibrium, the dynamics for one variable (X_k) of the nonlinear system 2.1 can be approximated by the corresponding linear system,

$$\frac{dx_k}{dt} = \left(\frac{\partial f_k}{\partial X_1}\bigg|_{\vec{X}^0}\right) x_1 + \left(\frac{\partial f_k}{\partial X_2}\bigg|_{\vec{X}^0}\right) x_2 + \cdots + \left(\frac{\partial f_k}{\partial X_n}\bigg|_{\vec{X}^0}\right) x_n + \sum_{j=1}^{m} B_{kj}\epsilon_{X,j}, \quad (2.2)$$

where x_k represent small deviations of the variable k from the equilibrium X_k^0; we evaluate the partial derivatives of the nonlinear function f_k at the equilibrium $\vec{X}^0$ (Guckenheimer & Holmes, 1983; Izhikevich, 2007), and we include the same stochastic perturbations as in the nonlinear system 2.1. We express the system 2.2 as

$$\frac{d}{dt}\vec{x} = \boldsymbol{A}\vec{x} + \boldsymbol{B}\vec{\epsilon}, \quad (2.3)$$

where $\vec{x}$ is the n-by-1 vector of deviations from the equilibrium, $\vec{\epsilon}$ is the m-by-1 vector of independent δ-correlated gaussian white noise sources, $\boldsymbol{A}$ is the n-by-n Jacobian matrix of the nonlinear system 2.1 evaluated at the equilibrium, and $\boldsymbol{B}$ is the n-by-m noise matrix,

$$\boldsymbol{B} = \begin{bmatrix} B_{11} & B_{12} & B_{13} & \ldots & B_{1m} \\ B_{21} & B_{22} & B_{23} & \ldots & B_{2m} \\ B_{31} & B_{32} & B_{33} & \ldots & B_{3m} \\ \vdots & \vdots & \vdots & \ddots & \vdots \\ B_{n1} & B_{n2} & B_{n3} & \ldots & B_{nm} \end{bmatrix},$$

where the parameter B_{ij} determines the contribution of noise source j to variable i. We assume that $\boldsymbol{A}$ satisfies the conditions required for the linear system 2.3 to accurately approximate the dynamics of the noise-free nonlinear system 2.1 near the equilibrium (i.e., we assume $\boldsymbol{A}$ has no eigenvalues with zero real part and the equilibrium is therefore hyperbolic (Guckenheimer & Holmes, 1983; Izhikevich, 2007).

For the linear system 2.3, the cross-spectral matrix $\boldsymbol{S}[\omega]$ can be obtained from the expression (Gardiner, 2004; Kleeman, 2011; Thomas & Lindner, 2019),

$$\boldsymbol{S}[\omega] = \frac{1}{2\pi}(\boldsymbol{A} + i\omega\boldsymbol{I})^{-1}(\boldsymbol{B}\,\boldsymbol{B}^T)(\boldsymbol{A}^T - i\omega\boldsymbol{I})^{-1}, \quad (2.4)$$

where $\boldsymbol{A}$ is real, $\boldsymbol{I}$ is the identity matrix, $i = \sqrt{-1}$, and $\omega = 2\pi f$ is the frequency. Evaluating the asymptotic behavior of the cross-spectral matrix at high frequencies (ω larger than any frequency associated with a natural rhythm of the linear system in equation 2.3), the spectrum of the observable variable X_1 is

$$S_{11}[\omega] = (B_{11}^2 + B_{12}^2 + \cdots + B_{1m}^2)\mathcal{O}(\omega^{-2}) + \mathcal{O}(\omega^{-4}), \tag{2.5}$$

where $\mathcal{O}(\omega^k)$ indicates the limiting behavior of the spectrum as a function of the kth power of ω as $\omega \to \infty$ (see the appendix).

The result in equation 2.5 shows that at high frequencies, the aperiodic exponent β depends on the relative noise to the observable variable. Without stochastic drive to the observable variable X_1 (i.e., with $B_{1k} = 0$ for all k in $\{1, 2, \ldots, m\}$),

$$S_{11}[\omega] = \mathcal{O}(\omega^{-4}),$$

so that the aperiodic exponent $\beta = -4$ at high frequencies (i.e., as $\omega \to \infty$). Alternatively, with stochastic drive to the observable variable X_1 (i.e., with $B_{1k} \neq 0$ for any k in $\{1, 2, \ldots m\}$),

$$S_{11}[\omega] = \mathcal{O}(\omega^{-2}),$$

so that the aperiodic exponent $\beta = -2$ at high frequencies (i.e., as $\omega \to \infty$). We note that in this case random walk dynamics dominate the spectrum at high frequencies, with well-known power-law behavior (Milotti, 2002).

To summarize, we consider a general, n-dimensional nonlinear dynamical system with stochastic drive, equation 2.1. We assume an equilibrium exists in this system with dynamics well approximated by the linearized system 2.2. Near this equilibrium, the dynamics produce aperiodic exponents between -4 and -2 at high frequencies (i.e., frequencies beyond the natural frequencies or spectral peaks of the system) consistent with the range of values observed in vivo. The value of the aperiodic exponent depends on the noise in the observed and latent variables; when noise in the observable variable X_1 dominates, the aperiodic exponent ≈ -2, while when the noise in the latent variables dominates, the aperiodic exponent ≈ -4.

The main result (see equation 2.5) and implications for the aperiodic exponent ($-4 \leq \beta \leq -2$) are for the general model, equation 2.1. These general results do not require a specific biophysical model of neural activity. In what follows, we illustrate the generality of these results in four example models, in which we choose the nonlinear functions f_k in model 2.1 and assume a square diagonal noise matrix $\boldsymbol{B}$ to simplify the presentation of numerical simulation results. In doing so, we show that each model produces

aperiodic exponents consistent with in vivo data ($-4 \leq \beta \leq -2$) but with different physical interpretations.

2.1 A Reduced Model of Single Neuron Activity. We first consider a reduced Hodgkin-Huxley type model (Hodgkin & Huxley, 1952; Izhikevich, 2007) to simulate the subthreshold dynamics of a single neuron. The model equations describe the dynamics of an observable voltage (V) and a latent membrane current (M),

$$\begin{aligned}\frac{dV}{dt} &= I_0 + g_M M(E_M - V) + \epsilon_V,\\ \frac{dM}{dt} &= \alpha_M[V](1 - M) - \beta_M[V]M + \epsilon_M.\end{aligned} \tag{2.6}$$

In the first equation, three terms drive the voltage dynamics: a constant input current (I_0), a dynamic membrane current ($g_M M(E_M - V)$), and voltage noise (ϵ_V, gaussian distributed with mean 0 and variance σ_V^2). In the second equation, the dynamics of the latent membrane current depend on forward ($\alpha_M[V]$) and backward ($\beta_M[V]$) rate functions,

$$\begin{aligned}\alpha_M[V] &= \frac{0.02}{1 + \exp\left(\frac{-V-20}{5}\right)},\\ \beta_M[V] &= 0.01 \exp\left(\frac{-V - 43}{18}\right).\end{aligned}$$

We choose these functions to simulate a muscarinic receptor suppressed potassium current (M-current; see Table A2 of Traub et al., 2003; see also Kopell et al., 2011, and Kramer, Roopun, et al., 2008). We omit other membrane currents (e.g., fast sodium and potassium currents) to focus on the subthreshold membrane dynamics without action potential generation. A stochastic drive also affects the membrane current dynamics (ϵ_M, gaussian distributed with mean 0 and variance σ_M^2).

Choosing the model parameters $I_0 = 1$, $g_M = 4$, and $E_M = -95$, we find an equilibrium of the noise-free model, equation 2.6, at

$$(V_0, M_0) \approx (-48.15, 0.00534).$$

The noise-driven linearized system near this equilibrium is approximately

$$\begin{aligned}\frac{d\overline{V}}{dt} &= -0.0213\,\overline{V} - 187.38\,\overline{M} + \epsilon_V,\\ \frac{d\overline{M}}{dt} &= 0.0000181\,\overline{V} - 0.0134\,\overline{M} + \epsilon_M,\end{aligned}$$

and the equilibrium is hyperbolic with eigenvalues $-0.0174 \pm 0.0581\,i$.

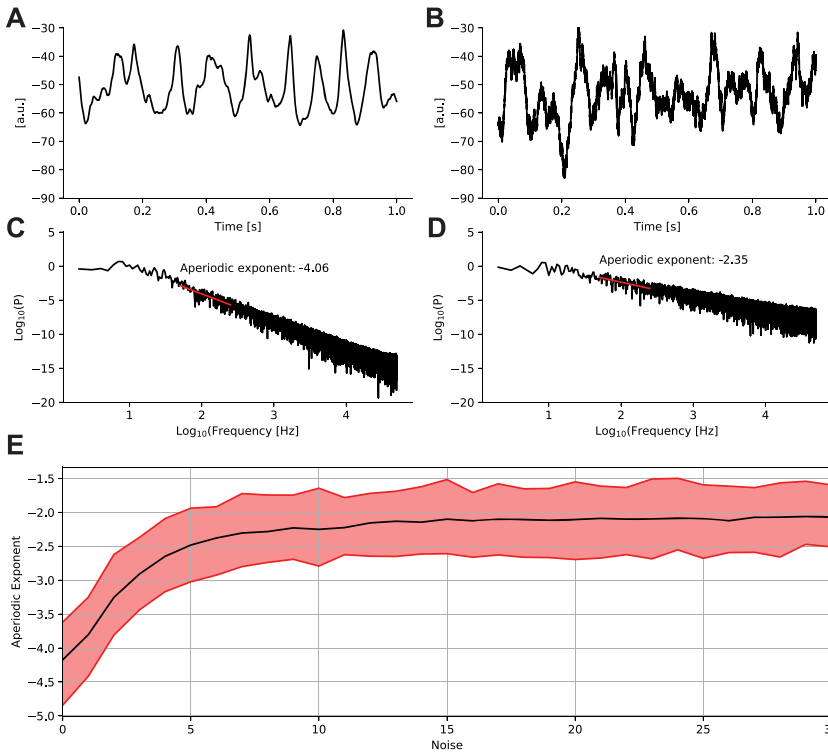

Figure 1: In a reduced model of single neuron activity, the aperiodic exponent increases from approximately -4 to -2 with the voltage noise. (A, B) Example voltage time series when (A) the voltage noise is 0 ($\epsilon_V = 0$), or (B) the voltage noise is nonzero ($\sigma_V = 20$). (C, D) The corresponding spectra (black) and linear fits (red, 50 Hz to 250 Hz) for the time series in panels A and B. (E) Estimates of the aperiodic exponent for increasing values of voltage noise. Black (red) indicates mean (standard deviation) of estimates across 100 simulations. In all simulations, the current noise ($\sigma_M = 0.01$) is fixed, and numerical integration is performed using the Euler–Maruyama method with time step 0.01 ms. Code to simulate the model and create this figure is available at https://github.com/Mark-Kramer/Aperiodic-Exponent-Model.

Consistent with the general theory, we expect this nonlinear Hodgkin-Huxley type model 2.6 to produce spectra with aperiodic exponents $-4 \leq \beta \leq -2$, depending on the values of the stochastic drives (ϵ_V, ϵ_M). To show this, we simulate the Hodgkin-Huxley type model, equation 2.6, and estimate the spectrum of the voltage variable V with fixed current noise ($\sigma_M = 0.01$) and variable voltage noise ($0 \leq \sigma_V \leq 30$). In agreement with the general theory (see Figure 1), as the voltage noise increases, the

aperiodic exponent increases from near $\beta \approx -4$ when $\sigma_V = 0$ to $\beta \approx -2$ when $\sigma_V = 30$.

We conclude that this nonlinear model of single neuron subthreshold dynamics, equation 2.6, produces aperiodic exponents consistent with the range of values observed in vivo. In agreement with the general theory, the value of the aperiodic exponent depends on the relative noise in the observable voltage variable and latent current variable. In this case, when noise in the membrane current dominates, the aperiodic exponent approaches -4; when noise in the voltage dominates, the aperiodic exponent approaches -2.

2.2 A Two-Dimensional Model of Neural Population Activity. We now consider the Wilson-Cowan equations as a model of neural population activity (Wilson & Cowan, 1972). The equations describe the interacting dynamics of an excitatory (E) and inhibitory (I) neural population,

$$\begin{aligned}\tau_e \frac{dE}{dt} &= -E + (k_e - r_e E)\, \mathcal{S}_e[c_1 E - c_2 I + P] + \epsilon_E,\\ \tau_i \frac{dI}{dt} &= -I + (k_i - r_i I)\, \mathcal{S}_i[c_3 E - c_4 I + Q] + \epsilon_I,\end{aligned} \tag{2.7}$$

where $\mathcal{S}$ is the sigmoid function,

$$\mathcal{S}_k[x] = \frac{1}{1 + \exp(-a_k(x - \theta_k))} - \frac{1}{1 + \exp(a_k\, \theta_k)},$$

and ϵ_E and ϵ_I are noise terms (gaussian distributed with mean 0 and variances σ_E^2 and σ_I^2, respectively). We choose the parameters to produce damped oscillatory behavior (see Figure 10 in Wilson & Cowan, 1972, and the caption of Figure 2 for the parameter values used here). With these parameters, we find an equilibrium of the noise-free model, equation 2.7,

$$(E_0, I_0) \approx (0.1511, 0.1585).$$

The noise-driven linearized system near this equilibrium is approximately

$$\begin{aligned}\frac{d\overline{E}}{dt} &= 1.482\, \overline{E} - 2.660\, \bar{I} + \epsilon_E,\\ \frac{d\bar{I}}{dt} &= 3.963\, \overline{E} - 1.981\, \bar{I} + \epsilon_I,\end{aligned}$$

and the equilibrium is hyperbolic, with eigenvalues $-0.250 \pm 2.75\, i$.

According to the general theory, we expect the nonlinear system, equation 2.7, near the equilibrium (E_0, I_0) to produce spectra with aperiodic exponents $-4 \le \beta \le -2$, depending on the values of the stochastic drives

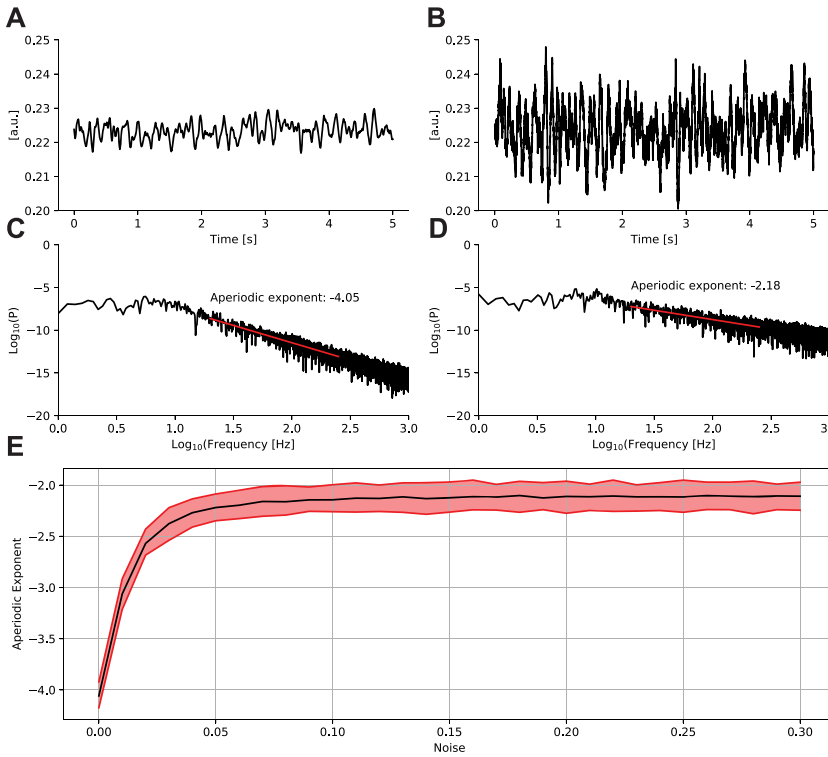

Figure 2: In a two-dimensional model of neural population activity, the aperiodic exponent increases from approximately -4 to -2 with the excitatory noise. (A, B) Example excitatory population time series when (A) the excitatory noise is 0 ($\epsilon_{\mathrm{E}} = 0$), or (B) the excitatory noise is nonzero ($\sigma_{\mathrm{E}} = 0.2$). (C, D) The corresponding spectra (black) and linear fits (red, 20–250 Hz) for the time series in panels A and B. (E) Estimates of the aperiodic exponent for increasing values of excitatory noise. Black (red) indicates mean (standard deviation) of estimates across 100 simulations. In all simulations, the inhibitory noise ($\sigma_{\mathrm{I}} = 0.1$) is fixed. We use these model parameters: $\mathrm{c}_1 = 15$, $\mathrm{c}_2 = 15$, $\mathrm{c}_3 = 15$, $\mathrm{c}_4 = 7$, $\mathrm{a}_{\mathrm{e}} = 1$, $\theta_{\mathrm{e}} = 2$, $\mathrm{a}_{\mathrm{i}} = 2$, $\theta_{\mathrm{i}} = 2.5$, $\tau_{\mathrm{e}} = 50$, $\tau_{\mathrm{i}} = 50$, $\mathrm{r}_{\mathrm{e}} = 1$, $\mathrm{r}_{\mathrm{i}} = 1$, $\mathrm{k}_{\mathrm{e}} = 1$, $\mathrm{k}_{\mathrm{i}} = 1$, $P = 1.25$, $Q = 0$. We perform numerical integration using the Euler–Maruyama method with time step 0.1 ms. Code to simulate the model and create this figure is available at https://github.com/Mark-Kramer/Aperiodic-Exponent-Model.

(ϵ_E, ϵ_I). To show this, we simulate the nonlinear system 2.7 and estimate the spectrum of the excitatory variable E with fixed inhibitory noise ($\sigma_I = 0.1$) and variable excitatory noise ($0 \leq \sigma_E \leq 0.3$). In agreement with the general theory (see Figure 2), as the excitatory noise increases, the aperiodic exponent increases from near $\beta \approx -4$ when $\sigma_E = 0$ to $\beta \approx -2$ when $\sigma_E = 0.3$.

We conclude that this nonlinear model of neural population activity, equation 2.7, produces aperiodic exponents consistent with the range of values observed in vivo. In this model, the value of the aperiodic exponent depends on the relative noise in the observable variable E and latent variable I. When noise in the inhibitory population dominates, the aperiodic exponent approaches -4; when noise in the excitatory population dominates, the aperiodic exponent approaches -2.

2.3 A 10-Dimensional Model of Neural Population Activity. To illustrate an application of the main result, equation 2.5, to a higher-dimensional neural model, we consider a mean-field model of neural population activity consisting of the coupled differential equations:

$$\tau_k \frac{dh_k}{dt} = (h_k^{rest} - h_k) + \psi_{ek}[h_e]I_{ek} + \psi_{ik}[h_i]I_{ik}$$
$$\left(\frac{d}{dt} + \gamma_k\right)^2 I_{kl} = (N_{kl}^{\beta} S_k[h_k] + P_{kl})G_k \gamma_k e, \tag{2.8}$$

where $k = \{e, i\}$ and $l = \{e, i\}$ denote excitatory (e) and inhibitory (i) neural populations, ψ_{kl} are normalized weighting functions, and $S_k[h_k]$ are sigmoidal transfer functions (Steyn-Ross et al., 2003). The model variables simulate the macrocolumn-averaged transmembrane soma voltage of an excitatory (h_e) and inhibitory (h_i) neural population, and synaptic input (I_{kl}) from population k to population l. Expressing the second-order differential equations for the synaptic inputs I_{kl} as first-order differential equations results in a system of 10 coupled first-order differential equations. The variable h_e is observable (Steyn-Ross et al., 1999) and the other variables are latent. We include independent stochastic drive to the dynamics of the observable variable (mean 0 and variance $\sigma_{h_e}^2$) and each latent variable (mean and variance σ_L^2 to all latent variables). Applications of the model include simulating electroencephalogram (EEG) dynamics during sleep (D. Steyn-Ross et al., 2005; Steyn-Ross et al., 2005; Wilson, Steyn-Ross, et al., 2006) seizures (Kramer et al., 2005, 2007; Steyn-Ross et al., 2012; Wilson, Sleigh, et al., 2006), and anesthesia (Steyn-Ross et al., 1999, 2003).

Fixing all model parameters to the default values in Steyn-Ross et al. (2003), a stable equilibrium exists (Steyn-Ross et al., 2003). We therefore expect, consistent with the general theory, model 2.8, to produce spectra with aperiodic exponents $-4 \leq \beta \leq -2$, depending on the values of the stochastic drives. To show this, we simulate the model 2.8 and estimate the spectrum of the voltage variable h_e with fixed noise ($\sigma_L = 50$) to all latent variables and variable noise to the observable variable (h_e, $0 \leq \sigma_{h_e} \leq 1$). In agreement with the general theory (see Figure 3), as the noise to the excitatory neural population increases, the aperiodic exponent increases from near $\beta \approx -4$ when $\sigma_{h_e} = 0$ to $\beta \approx -2$ when $\sigma_{h_e} = 1$.

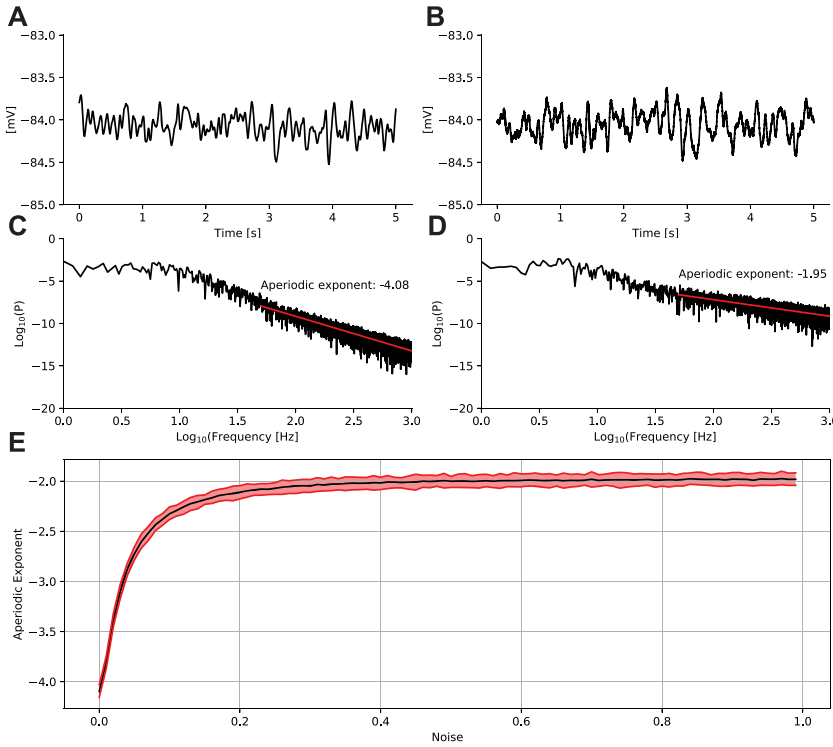

Figure 3: In a 10-dimensional model of neural population activity, the aperiodic exponent increases from approximately -4 to -2 with increasing noise to the excitatory neural population. (A, B) Example excitatory neural population activity when (A) noise to the excitatory neural population is 0 ($\epsilon_{h_e} = 0$) or (B) nonzero ($\sigma_{h_e} = 1$). (C, D) The corresponding spectra (black) and linear fits (red, 50 Hz–1000 Hz) for the time series in panels A and B. (E) Estimates of the aperiodic exponent for increasing values of excitatory neural population noise. Black (red) indicates mean (standard deviation) of estimates across 100 simulations. In all simulations, the latent noise terms ($\sigma_L = 50$) are fixed and numerical integration performed using the Euler–Maruyama method with time step 0.1 ms. Code to simulate the model and create this figure is available at https://github.com/Mark-Kramer/Aperiodic-Exponent-Model.

We conclude that this high-dimensional (10th order) nonlinear model of macroscopic neural population activity, equation 2.8, produces aperiodic exponents consistent with the range of values observed in vivo. In agreement with the general theory, the value of the aperiodic exponent depends on the relative noise in the observable variable (h_e) and latent variables. In this case, when noise outside the excitatory population dominates, the

aperiodic exponent approaches −4; when noise in the excitatory population (h_e) dominates, the aperiodic exponent approaches −2.

2.4 A Model of Predator-Prey Interactions. To illustrate the generality of the main result, equation 2.5, beyond models of neural activity we consider a nonlinear model of predator-prey interactions,

$$\frac{dx}{dt} = \frac{x(\gamma - x)}{\gamma} - x\,y + \epsilon_x,$$
$$\frac{dy}{dt} = -\alpha\,y + x\,y + \epsilon_y, \tag{2.9}$$

where x and y represent prey and predator populations, respectively, and the prey population includes self-regulation; (α, γ) are positive constants; and ϵ_x and ϵ_y are noise terms (gaussian distributed with mean 0 and variances σ_X^2 and σ_Y^2, respectively; Edelstein-Keshet, 2005). The nontrivial equilibrium of the deterministic system is

$$(x_0, y_0) = \left(\alpha, 1 - \frac{\alpha}{\gamma}\right),$$

and we require $\gamma > \alpha$ so that the equilibrium predator population is positive. The linearized system near this equilibrium is

$$\frac{d}{dt}\begin{pmatrix}\bar{x}\\ \bar{y}\end{pmatrix} = \boldsymbol{A}\begin{pmatrix}\bar{x}\\ \bar{y}\end{pmatrix} + \begin{pmatrix}\epsilon_x\\ \epsilon_y\end{pmatrix},$$

where $\boldsymbol{A} = \begin{pmatrix} -\frac{\alpha}{\gamma} & -\alpha \\ 1 - \frac{\alpha}{\gamma} & 0 \end{pmatrix}$. Because the trace of $\boldsymbol{A} = -\frac{\alpha}{\gamma}$ is negative, and the determinant of $\boldsymbol{A} = \alpha y_0$ is positive, the equilibrium is stable and hyperbolic (Edelstein-Keshet, 2005).

Consistent with the general theory, we expect this predator-prey model, equation 2.9, to produce spectra with aperiodic exponents $-4 \le \beta \le -2$, depending on the values of the stochastic drives (ϵ_x, ϵ_y). To show this, we simulate the predator-prey model, equation 2.9, over a range of parameters (α, γ) and estimate the spectrum of the prey variable x with fixed predator noise ($\sigma_y = 1$) and variable prey noise ($0 \le \sigma_x \le 0.005$). In agreement with the general theory, the values of the aperiodic exponent in this nonneural model lie within the range $-4 \le \beta \le -2$, depending on the relative noise in the prey variable (see Figure 4). As the prey noise increases, the aperiodic exponent increases from near $\beta \approx -4$ when $\sigma_x = 0$ to $\beta \approx -2$ when $\sigma_x = 0.005$ across a range of model parameters (α, γ).

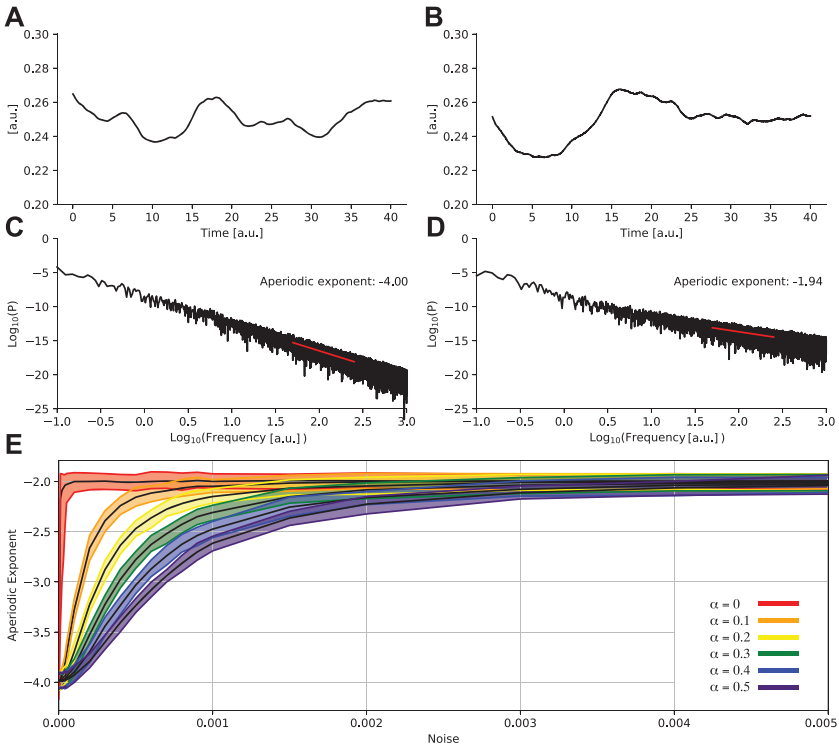

Figure 4: In a predator-prey population model, the aperiodic exponent increases from approximately -4 to -2 with the prey noise. (A, B) Example prey population dynamics when (A) the prey noise is 0 ($\epsilon_x = 0$) or (B) the prey noise is nonzero ($\sigma_x = 0.01$). (C, D) The corresponding spectra (black) and linear fits (red, 50–250 Hz) for the time series in panels A and B. (E) Estimates of the aperiodic exponent for increasing values of prey noise. Black (color) indicates mean (standard deviation) of estimates across 100 simulations. In all simulations, the predator noise ($\sigma_y = 1$) is fixed, and the model simulated for 250,000 steps with numerical integration performed using the Euler–Maruyama method with time step 0.0002 a.u; to avoid an initial large amplitude transient, we omit the first 50,000 steps of simulated data from analysis. In panels A to D, the parameters are $\alpha = 0.25$, $\gamma = 0.6$. In panel E, colors indicate simulations at $\alpha = \{0.0, 0.1, \ldots, 0.5\}$. For each fixed α, we simulate 10 instances of the model at 10 different values of $\gamma = \{0.1, 0.2, 0.3, \ldots, 1.0\}$ for a total of 100 simulations. Code to simulate the model and create this figure is available at https://github.com/Mark-Kramer/Aperiodic-Exponent-Model.

We note that, mathematically, three of the four models are essentially the same; the Hodgkin-Huxley type model, equation 2.6; the two-dimensional neural population model, equation 2.7; and the predator-prey model,

equation 2.9, are all planar models with independent additive noise in the two variables. We choose to illustrate the theory with these example simulations to demonstrate the difficulty of interpreting the biological mechanism producing the aperiodic exponent. While the four models, equations 2.6 to 2.9, simulate different neural and nonneural dynamics, each model produces 1/f-like scaling with aperiodic exponents consistent with in vivo observations of neural activity. The interpretation of the mechanism affecting the aperiodic exponent depends on the model choice; the aperiodic exponent β approaches -2 with increasing voltage noise in equation 2.6, noise to an excitatory neural population in equations 2.7 and 2.8, or prey noise in equation 2.9. Because each model satisfies the general conditions (i.e., a hyperbolic equilibrium exists), the spectral results derived for the general model in equation 2.5 capture the 1/f-like spectrum for each specific, biophysical model considered here.

3 Discussion

A universal feature of neural field potential spectra is 1/f-like scaling at high frequencies. To produce this power law, many generative mechanisms have been proposed with diverse biological implementations and interpretations. Here, we do not propose that a specific biological mechanism produces 1/f-like scaling. Instead, to understand how different neural mechanisms can produce similar 1/f-like scaling, we consider a general nonlinear dynamical system with stochastic drive. We show that dynamics near a (hyperbolic) equilibrium in this general model of neural activity produce aperiodic exponents between -4 and -2, consistent with the range of values reported in vivo for higher frequencies (e.g., >20 Hz). We illustrate these results in neural and nonneural models. We propose that the range of aperiodic exponents observed across recording modalities, experiments, and neural systems is a natural consequence of a noise-driven dynamical system.

We considered here a single statistic, the aperiodic exponent, reflecting the 1/f-like feature of the neural field spectrum. We note that many different models can explain the same observed statistic. For example, observations from neural systems can produce spectra with broadband peaks in the gamma band (approximately 30–80 Hz; Fries et al., 2007). Many approaches exist to explain these observed spectral peaks, including statistical approaches (e.g., an autoregressive model of order two; Spyropoulos et al., 2020), mechanical approaches (e.g., a damped driven oscillator; Spyropoulos et al., 2020), or biophysical approaches (e.g., the interneuron network model, or the pyramidal-interneuron network model; Whittington et al., 2000). Our understanding of the gamma rhythm in a particular experiment depends on the model choice. In the same way, observations from neural systems produce spectra with 1/f-like scaling at high frequencies, and many models exist to explain this scaling. Our results show

mathematically why many models can produce the range of aperiodic exponents observed in vivo ($-4 \leq \beta \leq -2$). Due to the general nature of this mathematical result, it is not surprising that many different proposals exist to explain the 1/f-like spectrum. In practice, we expect that biological mechanisms must exist to create the scaling observed in vivo. Identifying these biological mechanisms and their expression in the diverse observations of 1/f-like scaling reported remains an important challenge.

Our results are consistent with previous work showing that power-law scaling occurs in simple stochastic or physical systems. For example, Gao et al. (2017) relate estimates of the aperiodic exponent to changes in the balance between excitation and inhibition. To do so, they simulate the local field potential as the summed synaptic current generated by independent stochastic spiking excitatory and inhibitory cells. Bédard et al. (2006) propose that 1/f-like scaling in the spectrum does not rely on critical states but instead depends on the filtering properties of the extracellular medium (although this mechanism remains debated; Logothetis et al., 2007). Touboul and Destexhe (2010) show that simple models of stochastic processes (high-frequency shot-noise processes or Ornstein-Uhlenbeck processes) produce peak-amplitude distributions consistent with power-law distributions. Priesemann and Shriki (2018) show that inhomogeneous Poisson processes can produce approximate power law distributions in the size and duration distributions of avalanches (i.e., activity cascades). Consistent with our results, these examples generate power-law scaling without requiring a sophisticated biological or mathematical mechanism. Distinct from these previous works, we consider an (unspecified) n-dimensional dynamical system and show that, near a (hyperbolic) equilibrium, stochastic drive produces aperiodic exponents consistent with values observed in vivo.

Under the general framework considered here, the range of aperiodic exponents reflects different types of noise. The observable dynamics (e.g., variable X_1 in equation 2.1) depend directly on the stochastic drives to the observable variable, and indirectly on the stochastic drives to the latent variable(s). The latent dynamics introduce correlations in the uncorrelated latent noise process before this noise reaches the observable dynamics. Therefore, the observable dynamics depend on both uncorrelated and correlated noise inputs, and we may interpret the aperiodic exponent in terms of these different types of noise; an aperiodic exponent near $\beta = -4$ indicates that correlated noise inputs dominate the high-frequency observable dynamics, while $\beta = -2$ indicates that uncorrelated noise dominates the high-frequency observable dynamics. These general results are independent of a specific biophysical mechanism, and a biophysical interpretation of the relationship between different types of noise and the aperiodic exponent depends on the specific model choice.

Some observations report aperiodic exponents greater than -2 (i.e., $\beta > -2$), beyond the range of aperiodic exponents derived here. Experimental

factors, such as measurement noise, which flattens the spectrum and shifts β toward 0, might contribute to these observations. In addition, analysis factors may affect reported results. For example, the frequency range considered varies widely across studies (see the discussion of fitting ranges in Gerster et al., 2022). In general, larger aperiodic exponents (more negative β) occur at higher frequencies (Bédard et al., 2006; Colombo et al., 2019; Ibarra Chaoul & Siegel, 2021; Racz et al., 2021), although not always (Chaudhuri et al., 2018). In the framework considered here, the result $-4 \leq \beta \leq -2$ holds in the high-frequency limit (when the measured frequency exceeds any natural frequency of the neural population) and near an equilibrium of the dynamical system. In lower-frequency bands (e.g., below the natural frequency), our simplifying asymptotic arguments no longer apply, and the relationship between power and frequency will depend on the model parameters. In addition, we note that the aperiodic exponent reported in lower-frequency bands is more difficult to interpret. To assess low-frequency rhythms requires long durations of data, which increases the chance of nonstationarity. Artifacts (e.g., slow drifts) and analysis choices (e.g., whether to subtract the signal mean) also affect the low-frequency power. Finally, while power-law features at low frequencies may reflect the same power-law features at high frequencies, these different phenomena unlikely reflect the same neural mechanisms. We also expect analyzing dynamics away from an equilibrium of the dynamical system will increase the aperiodic exponent. Away from an equilibrium, nonlinear terms in the model have a greater impact on the dynamics and the resulting spectrum. These nonlinearities may increase power at high frequencies (e.g., Kramer et al., 2008) and therefore increase the aperiodic exponent beyond the range derived for the linear dynamics near the equilibrium.

Here we considered additive gaussian noise as the stochastic inputs to the dynamical models. However, alternative noise sources would provide more accurate approximations of biological systems. For example, for conductance-based neural models, more biophysically plausible noise sources would include noise in the membrane current dynamics with variance proportional to the opening and closing rates of ion channels (Pu & Thomas, 2020, 2021). For models of neural population activity, stochastic perturbations may be scaled by the square root of the population size (Benayoun et al., 2010; Candia et al., 2021). For models of ecological population dynamics, noise may be scaled proportional to the birth and death rates (Barendregt & Thomas, 2023; Huynh et al., 2023; Strang et al., 2019). Understanding the impact of more biologically realistic noise (e.g., state-dependent noise) on the power-law behavior remains an important topic for future investigation.

Many well-supported observations of power laws appear in neuroscience, including avalanches of population voltage discharges (Beggs & Plenz, 2003) and amplitudes of narrowband oscillations (Linkenkaer-Hansen et al., 2001). Here, we consider one type of power law: the 1/f-like

neural field spectrum and a general, noise-driven dynamical system. Under this general model, the aperiodic exponent represents the impact of noise in the observable and latent dynamics, without requiring a sophisticated biological or dynamical mechanism. We propose that the range of aperiodic exponents $-4 \le \beta \le -2$ observed in vivo represents the expected dynamics near an equilibrium in a nonlinear dynamical system driven by noise. The generality of the model is consistent with the universality of 1/f-like field spectra, reflecting a basic dynamical feature present in many different neural systems. However, this simplicity may also limit the computational utility of this mechanism and the role of the aperiodic exponent in measuring neural computations.

4 Materials and Methods

To estimate the aperiodic exponent β, we first compute the spectrum in the standard way. To a simulated voltage time series (V_t) with sampling interval Δ and duration T, we subtract the mean, apply a Hanning taper, compute the Fourier transform (V_f), and multiply by the complex conjugate (V_f^*):

$$P = \frac{2\Delta^2}{T} V_f V_f^*.$$

We note that the square of the Fourier coefficients is essential for consistent interpretation of the aperiodic exponent across studies; omitting the square is a common mistake identified in previous work (see the discussion in Milotti, 2002). For frequencies f, we fit a linear model to the logarithm base 10 of the spectrum ($\log_{10} P$) with predictor logarithm base 10 of the frequency ($\log_{10} f$),

$$\log_{10} P = c + \beta \log_{10} f,$$

where β is the estimate of the aperiodic exponent. Code to compute the spectrum and estimate the aperiodic exponent is available at https://github.com/Mark-Kramer/Aperiodic-Exponent-Model.

Appendix: Derivation of the Asymptotic Behavior of the Cross-Spectral Matrix

Consider the two terms of equation 2.4 that involve the Jacobian,

$$(\boldsymbol{A} + i\omega \boldsymbol{I})^{-1} \text{ and } (\boldsymbol{A}^T - i\omega \boldsymbol{I})^{-1}.$$

In general, these n-by-n matrices are complicated expressions of the constants in $\boldsymbol{A}$ and powers of ω. To characterize the limiting behavior of these

matrices for large values of ω, we express each of these two terms using asymptotic notation,

$$\begin{bmatrix} \mathcal{O}(\omega^{-1}) & \mathcal{O}(\omega^{-2}) & \mathcal{O}(\omega^{-2}) & \cdots & \mathcal{O}(\omega^{-2}) \\ \mathcal{O}(\omega^{-2}) & \mathcal{O}(\omega^{-1}) & \mathcal{O}(\omega^{-2}) & \cdots & \mathcal{O}(\omega^{-2}) \\ \mathcal{O}(\omega^{-2}) & \mathcal{O}(\omega^{-2}) & \mathcal{O}(\omega^{-1}) & \cdots & \mathcal{O}(\omega^{-2}) \\ \vdots & \vdots & \vdots & \ddots & \vdots \\ \mathcal{O}(\omega^{-2}) & \mathcal{O}(\omega^{-2}) & \mathcal{O}(\omega^{-2}) & \cdots & \mathcal{O}(\omega^{-1}) \end{bmatrix},$$

where terms on the diagonal grow proportional to ω^{-1} and terms off the diagonal grow proportional to ω^{-2} as $\omega \to \infty$. The noise matrix $\boldsymbol{B}$ enters the calculation only as a symmetric matrix $\boldsymbol{D}$,

$$\boldsymbol{D} = \boldsymbol{B}\,\boldsymbol{B}^T = \begin{bmatrix} D_{11} & D_{12} & D_{13} & \ldots & D_{1n} \\ D_{12} & D_{22} & D_{23} & \ldots & D_{2n} \\ D_{13} & D_{23} & D_{33} & \ldots & D_{3n} \\ \vdots & \vdots & \vdots & \ddots & \vdots \\ D_{1n} & D_{2n} & D_{3n} & \ldots & D_{nn} \end{bmatrix},$$

and we note $D_{11} = B_{11}^2 + B_{12}^2 + \ldots + B_{1m}^2$, the sum of each squared element in the first row of $\boldsymbol{B}$. The first row of

$$(\boldsymbol{A} + i\omega\boldsymbol{I})^{-1}\boldsymbol{D}$$

then becomes

$$\begin{aligned} &[D_{11}\mathcal{O}(\omega^{-1}) + (D_{12} + D_{13} + \cdots + D_{1n})\mathcal{O}(\omega^{-2}), \\ &D_{12}\mathcal{O}(\omega^{-1}) + (D_{22} + D_{23} + \cdots + D_{2n})\mathcal{O}(\omega^{-2}), \\ &D_{13}\mathcal{O}(\omega^{-1}) + (D_{23} + D_{33} + \cdots + D_{3n})\mathcal{O}(\omega^{-2}), \\ &\qquad\qquad\vdots \\ &D_{1n}\mathcal{O}(\omega^{-1}) + (D_{2n} + D_{3n} + \cdots + D_{nn})\mathcal{O}(\omega^{-2})]. \end{aligned}$$

To determine the spectrum of the observable variable ($S_{11}[\omega]$), we compute the first entry of the cross-spectral matrix $\boldsymbol{S}[\omega]$ in equation 2.4,

$$(\boldsymbol{A} + i\omega\boldsymbol{I})^{-1}\boldsymbol{D}\,(\boldsymbol{A}^T - i\omega\boldsymbol{I})^{-1},$$

which corresponds to multiplying the two vectors,

$$\begin{matrix}
[D_{11}\mathcal{O}(\omega^{-1}) + (D_{12} + D_{13} + \cdots + D_{1n})\mathcal{O}(\omega^{-2}), & & [\mathcal{O}(\omega^{-1}), \\
D_{12}\mathcal{O}(\omega^{-1}) + (D_{22} + D_{23} + \cdots + D_{2n})\mathcal{O}(\omega^{-2}), & & \mathcal{O}(\omega^{-2}), \\
D_{13}\mathcal{O}(\omega^{-1}) + (D_{23} + D_{33} + \cdots + D_{3n})\mathcal{O}(\omega^{-2}), & \text{and} & \mathcal{O}(\omega^{-2}), \\
\vdots & & \vdots \\
D_{1n}\mathcal{O}(\omega^{-1}) + (D_{2n} + D_{3n} + \cdots + D_{nn})\mathcal{O}(\omega^{-2})] & & \mathcal{O}(\omega^{-2})]
\end{matrix}$$

element by element. Doing so, we find,

$$S_{11}[\omega] = D_{11}\mathcal{O}(\omega^{-2}) + \mathcal{O}(\omega^{-4}),$$

or

$$S_{11}[\omega] = (B_{11}^2 + B_{12}^2 + \cdots + B_{1m}^2)\mathcal{O}(\omega^{-2}) + \mathcal{O}(\omega^{-4}), \tag{A.1}$$

where we note that the $\mathcal{O}(\omega^{-3})$ terms vanish due to the symmetry of $\boldsymbol{D}$.

To illustrate these general results, we consider a two-dimensional dynamical system with

$$\boldsymbol{A} = \begin{pmatrix} a & b \\ c & d \end{pmatrix} \quad \text{and} \quad \boldsymbol{B} = \begin{pmatrix} B_{11} & B_{12} \\ B_{21} & B_{22} \end{pmatrix}.$$

Evaluating the cross-spectral matrix, equation 2.4, for the observable variable ($S_{XX}[\omega]$), we find

$$S_{XX}[\omega] = \frac{1}{2\,\pi}\,\frac{b^2(B_{21}^2 + B_{22}^2) - 2\,b\,d(B_{11}B_{21} + B_{12}B_{22}) + (B_{11}^2 + B_{12}^2)(d^2 + \omega^2)}{(b\,c - a\,d)^2 + (a^2 + 2\,b\,c + d^2)\omega^2 + \omega^4}. \tag{A.2}$$

Isolating the ω^2 term in the numerator, this expression becomes,

$$S_{XX}[\omega] = \frac{\mathcal{O}(1) + (B_{11}^2 + B_{12}^2)\mathcal{O}(\omega^2)}{\mathcal{O}(\omega^4)} = (B_{11}^2 + B_{12}^2)\mathcal{O}(\omega^{-2}) + \mathcal{O}(\omega^{-4})$$

as $\omega \to \infty$, equivalent to the general expression A.1.

To illustrate the cross-spectral matrix $S_{XX}[\omega]$ for a specific two-dimensional dynamical system, we consider the predator-prey model, equation 2.9. In this case, $B_{11} = \sigma_x$, $B_{12} = B_{21} = 0$, and $B_{22} = \sigma_y = 1$, so that equation A.2 becomes

$$S_{XX}[\omega] = \frac{1}{2\,\pi}\,\frac{b^2 + \sigma_x^2(d^2 + \omega^2)}{(b\,c - a\,d)^2 + (a^2 + 2\,b\,c + d^2)\omega^2 + \omega^4}.$$

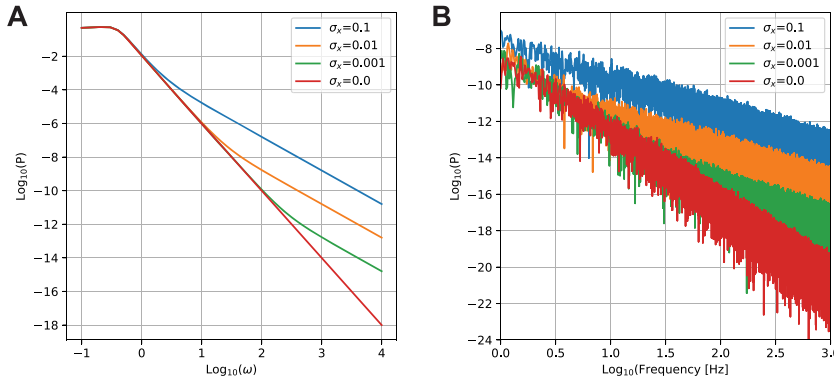

Figure 5: Analytic and estimated spectra for the predator-prey model. (A) The analytic spectrum, equation A.3, for the prey variable at different values of prey noise (σ_x, see legend). When prey noise is 0, the aperiodic exponent is -4 at high frequencies (red curve). As the prey noise increases, a knee appears in the curve, and the aperiodic exponent becomes -2 at high frequencies. (B) Spectra estimated from numerical simulations of the predator-prey model at the same values of prey noise (σ_x; see the legend). The shift to an aperiodic exponent of -2 at high frequencies becomes difficult to detect. For all curves, we fix $\alpha = 0.25$, $\gamma = 0.6$, and $\sigma_y = 1$ and perform numerical integration using the Euler–Maruyama method with time step 0.0002 a.u. Code to create this figure is available at https://github.com/Mark-Kramer/Aperiodic-Exponent-Model.

Fixing $\alpha = 0.25$ and $\gamma = 0.6$ as in Figures 4A to 4D, we find

$$a = -\frac{0.25}{0.6}, \quad b = -0.25, \quad c = 1 - \frac{0.25}{0.6}, \quad d = 0,$$

so that the cross-spectrum for the observable (prey) variable becomes

$$S_{XX}[\omega] = \frac{1}{2\,\pi}\left(\frac{\sigma_x^2\omega^2}{0.0212674 - 0.118056\,\omega^2 + \omega^4} + \frac{0.0625}{0.0212674 - 0.118056\,\omega^2 + \omega^4}\right). \tag{A.3}$$

We show in Figure 5A this cross-spectrum for different values of prey noise (σ_x). When $\sigma_x = 0$, the first term in equation A.3 is zero and the ω^{-4} term dominates the spectrum (red curve in Figure 5A). When σ_x increases to 0.001, the first term in equation A.3 becomes nonzero and the ω^{-2} term affects the spectrum. However, because σ_x is small, the effect of the ω^{-2} term appears only at large ω, where the second term of $S_{XX}[\omega]$ in equation A.3 is small (green curve in Figure 5A). As σ_x increases, the impact of the first

(ω^{-2}) term increases and emerges above the second (ω^{-4}) term at lower frequencies (orange and blue curves in Figure 5A). A knee in the curve occurs at the transition from ω^{-4} behavior (at lower frequencies) to ω^{-2} behavior (at higher frequencies). We note that estimating a single aperiodic exponent over the high-frequency range produces a single estimate for the slope of $S_{XX}[\omega]$; a more representative approach would instead identify the knee in the curve and estimate the two separate slopes. However, in practice, noisy spectral estimates from time series data obfuscate this change in aperiodic exponent (see the examples in Figure 5B).

Acknowledgments

We thank Konstantinos Spiliopoulos and Uri Eden for recommendations regarding the analysis of stochastic differential equations. We were supported in part by NSF 1451384, NIH R01NS110669, and NIH R01NS119483.

References

Adelhöfer, N., Paulus, T., Mückschel, M., Bäumer, T., Bluschke, A., Takacs, A., . . . Beste, C. (2021). Increased scale-free and aperiodic neural activity during sensorimotor integration—A novel facet in Tourette syndrome. *Brain Communications*, *3*(4), fcab250. 10.1093/braincomms/fcab250

Bak, P., Tang, C., & Wiesenfeld, K. (1987). Self-organized criticality: An explanation of the 1/*f* noise. *Physical Review Letters*, *59*(4), 381–384. 10.1103/PhysRevLett.59.381

Barendregt, N. W., & Thomas, P. J. (2023). Heteroclinic cycling and extinction in May–Leonard models with demographic stochasticity. *Journal of Mathematical Biology*, *86*(2), 30. 10.1007/s00285-022-01859-4

Bédard, C., & Destexhe, A. (2008). A modified cable formalism for modeling neuronal membranes at high frequencies. *Biophysical Journal*, *94*(4), 1133–1143. 10.1529/biophysj.107.113571

Bédard, C., Kröger, H., & Destexhe, A. (2006). Does the 1/f frequency scaling of brain signals reflect self-organized critical states? *Physical Review Letters*, *97*(11), 118102.

Beggs, J. M., & Plenz, D. (2003). Neuronal avalanches in neocortical circuits. *Journal of Neuroscience*, *23*(35), 11167–11177. 10.1523/JNEUROSCI.23-35-11167.2003

Benayoun, M., Cowan, J. D., Drongelen, W. van, & Wallace, E. (2010). Avalanches in a stochastic model of spiking neurons. *PLOS Computational Biology*, *6*(7). e1000846. 10.1371/journal.pcbi.1000846

Bódizs, R., Szalárdy, O., Horváth, C., Ujma, P. P., Gombos, F., Simor, P., . . . Dresler, M. (2021). A set of composite, non-redundant EEG measures of NREM sleep based on the power law scaling of the Fourier spectrum. *Scientific Reports*, *11*(1), 2041. 10.1038/s41598-021-81230-7

Buzsaki, G. (2011). *Rhythms of the brain*. Oxford University Press.

Buzsáki, G., Anastassiou, C., & Koch, C. (2012). The origin of extracellular fields and currents—EEG, ECoG, LFP and spikes. *Nature Reviews Neuroscience*, *13*(6), 407–420. 10.1038/nrn3241

Buzsaki, G., & Draguhn, A. (2004). Neuronal oscillations in cortical networks. *Science*, *304*(5679), 1926–1929. 10.1126/science.1099745

Candia, A. de, Sarracino, A., Apicella, I., & Arcangelis, L. de. (2021). Critical behaviour of the stochastic Wilson-Cowan model. *PLOS Computational Biology*, *17*(8). e1008884. 10.1371/journal.pcbi.1008884

Cesnaite, E., Steinfath, P., Jamshidi Idaji, M., Stephani, T., Kumral, D., Haufe, S., . . . Nikulin, V. V. (2023). Alterations in rhythmic and non-rhythmic resting-state EEG activity and their link to cognition in older age. *NeuroImage*, *268*, 119810. 10.1016/j.neuroimage.2022.119810

Chaudhuri, R., He, B. J., & Wang, X.-J. (2018). Random recurrent networks near criticality capture the broadband power distribution of human ECoG dynamics. *Cerebral Cortex*, *28*(10), 3610–3622. 10.1093/cercor/bhx233

Cocchi, L., Gollo, L. L., Zalesky, A., & Breakspear, M. (2017). Criticality in the brain: A synthesis of neurobiology, models and cognition. *Progress in Neurobiology*, *158*, 132–152. 10.1016/j.pneurobio.2017.07.002

Colombo, M. A., Napolitani, M., Boly, M., Gosseries, O., Casarotto, S., Rosanova, M., . . . Sarasso, S. (2019). The spectral exponent of the resting EEG indexes the presence of consciousness during unresponsiveness induced by propofol, xenon, and ketamine. *NeuroImage*, *189*, 631–644. 10.1016/j.neuroimage.2019.01.024

Donoghue, T., Haller, M., Peterson, E. J., Varma, P., Sebastian, P., Gao, R., . . . Voytek, B. (2020). Parameterizing neural power spectra into periodic and aperiodic components. *Nature Neuroscience*, *23*(12), 1655–1665. 10.1038/s41593-020-00744-x

Edelstein-Keshet, L. (2005). *Mathematical models in biology*. SIAM.

Evertz, R., Hicks, D. G., & Liley, D. T. J. (2022). Alpha blocking and 1/fβ spectral scaling in resting EEG can be accounted for by a sum of damped alpha band oscillatory processes. *PLOS Computational Biology*, *18*(4), e1010012. 10.1371/journal.pcbi.1010012

Fransson, P., Metsäranta, M., Blennow, M., Åden, U., Lagercrantz, H., & Vanhatalo, S. (2013). Early development of spatial patterns of power-law frequency scaling in fMRI resting-state and EEG data in the newborn brain. *Cerebral Cortex*, *23*(3), 638–646. 10.1093/cercor/bhs047

Freeman, W. J., Rogers, L. J., Holmes, M. D., & Silbergeld, D. L. (2000). Spatial spectral analysis of human electrocorticograms including the alpha and gamma bands. *Journal of Neuroscience Methods*, *95*(2), 111–121. 10.1016/S0165-0270(99)00160-0

Freeman, W. J., & Zhai, J. (2009). Simulated power spectral density (PSD) of background electrocorticogram (ECoG). *Cognitive Neurodynamics*, *3*(1), 97–103. 10.1007/s11571-008-9064-y

Fries, P., Nikolić, D., & Singer, W. (2007). The gamma cycle. *Trends in Neurosciences*, *30*(7), 309–316. 10.1016/j.tins.2007.05.005

Gao, R., Peterson, E. J., & Voytek, B. (2017). Inferring synaptic excitation/inhibition balance from field potentials. *NeuroImage*, *158*, 70–78. 10.1016/j.neuroimage.2017.06.078

Gardiner, C. (2004). *Handbook of stochastic methods*. Springer-Verlag.

Gerster, M., Waterstraat, G., Litvak, V., Lehnertz, K., Schnitzler, A., Florin, E., . . . Nikulin, V. (2022). Separating neural oscillations from aperiodic 1/f activity: Challenges and recommendations. *Neuroinformatics*, *20*(4), 991–1012. 10.1007/s12021-022-09581-8

Gibbs, F., Gibbs, E., & Lennox, W. (2002). Epilepsy: A paroxysmal cerebral dysrhythmia. *Epilepsy and Behavior*, *3*(4), 395–401. 10.1016/S1525-5050(02)00050-1

Guckenheimer, J., & Holmes, P. (1983). *Nonlinear oscillations, dynamical systems, and bifurcations of vector fields*. Springer-Verlag.

He, B. J. (2014). Scale-free brain activity: Past, present, and future. *Trends in Cognitive Sciences*, *18*(9), 480–487. 10.1016/j.tics.2014.04.003

He, B. J., Zempel, J. M., Snyder, A. Z., & Raichle, M. E. (2010). The temporal structures and functional significance of scale-free brain activity. *Neuron*, *66*(3), 353–369. 10.1016/j.neuron.2010.04.020

Hodgkin, A. L., & Huxley, A. F. (1952). A quantitative description of membrane current and its application to conduction and excitation in nerve. *Journal of Physiology*, *117*(4), 500–544. 10.1113/jphysiol.1952.sp004764

Horváth, C. G., Szalárdy, O., Ujma, P. P., Simor, P., Gombos, F., Kovács, . . . Bódizs, R. (2022). Overnight dynamics in scale-free and oscillatory spectral parameters of NREM sleep EEG. *Scientific Reports*, *12*(1), art. 1.

Huynh, L., Scott, J. G., & Thomas, P. J. (2023). Inferring density-dependent population dynamics mechanisms through rate disambiguation for logistic birth-death processes. *Journal of Mathematical Biology*, *86*(4), 50. 10.1007/s00285-023-01877-w

Ibarra Chaoul, A., & Siegel, M. (2021). Cortical correlation structure of aperiodic neuronal population activity. *NeuroImage*, *245*, 118672. 10.1016/j.neuroimage.2021.118672

Izhikevich, E. (2007). *Dynamical systems in neuroscience*. MIT Press.

Jirsa, V. K. (2009). Neural field dynamics with local and global connectivity and time delay. *Philosophical Transactions Series A, Mathematical, Physical, and Engineering Sciences*, *367*(1891), 1131–1143. 10.1098/rsta.2008.0260

Kleeman, R. (2011). Spectral analysis of multidimensional stochastic geophysical models with an application to decadal ENSO variability. *Journal of the Atmospheric Sciences*, *68*(1), 13–25. 10.1175/2010JAS3546.1

Kopell, N., Whittington, M. A., & Kramer, M. A. (2011). Neuronal assembly dynamics in the beta1 frequency range permits short-term memory. *Proceedings of the National Academy of Sciences*, *108*(9), 3779–3784. 10.1073/pnas.1019676108

Kramer, M. A., Kirsch, H. E., & Szeri, A. J. (2005). Pathological pattern formation and cortical propagation of epileptic seizures. *Journal of the Royal Society Interface*, *2*(2), 113–127. 10.1098/rsif.2004.0028

Kramer, M. A., Roopun, A. K., Carracedo, L. M., Traub, R. D., Whittington, M. A., & Kopell, N. J. (2008). Rhythm generation through period concatenation in rat somatosensory cortex. *PLOS Computational Biology*, *4*(9), e1000169. 10.1371/journal.pcbi.1000169

Kramer, M. A., Szeri, A. J., Sleigh, J. W., & Kirsch, H. E. (2007). Mechanisms of seizure propagation in a cortical model. *Journal of Computational Neuroscience*, *22*(1), 63–80. 10.1007/s10827-006-9508-5

Kramer, M. A., Tort, A. B. L., & Kopell, N. J. (2008). Sharp edge artifacts and spurious coupling in EEG frequency comodulation measures. *Journal of Neuroscience Methods*, *170*(2), 352–357. 10.1016/j.jneumeth.2008.01.020

Lanzone, J., Colombo, M. A., Sarasso, S., Zappasodi, F., Rosanova, M., Massimini, M., . . . Assenza, G. (2022). EEG spectral exponent as a synthetic index for the

longitudinal assessment of stroke recovery. *Clinical Neurophysiology*, *137*, 92–101. 10.1016/j.clinph.2022.02.022

Lendner, J. D., Helfrich, R. F., Mander, B. A., Romundstad, L., Lin, J. J., Walker, M. P., . . . Knight, R. T. (2020). An electrophysiological marker of arousal level in humans. *eLife*, *9*, e55092. 10.7554/eLife.55092

Linkenkaer-Hansen, K., Nikouline, V. V., Palva, J. M., & Ilmoniemi, R. J. (2001). Long-range temporal correlations and scaling behavior in human brain oscillations. *Journal of Neuroscience*, *21*(4), 1370–1377. 10.1523/JNEUROSCI.21-04-01370.2001

Logothetis, N. K., Kayser, C., & Oeltermann, A. (2007). In vivo measurement of cortical impedance spectrum in monkeys: Implications for signal propagation. *Neuron*, *55*(5), 809–823. 10.1016/j.neuron.2007.07.027

Miller, K., Sorensen, L., Ojemann, J., & den Nijs, M. (2009). Power-law scaling in the brain surface electric potential. *PLOS Computational Biology*, *5*(12), e1000609 EP. 10.1371/journal.pcbi.1000609

Milotti, E. (2002). *1/f noise: A pedagogical review*. http://arxiv.org/abs/physics/0204033

Milstein, J., Mormann, F., Fried, I., & Koch, C. (2009). Neuronal shot noise and Brownian 1/f2 behavior in the local field potential. *PLOS One 4*(2), e4338. 10.1371/journal.pone.0004338

Newman, M. (2005). Power laws, Pareto distributions and Zipf's law. *Contemporary Physics*, *46*(5), 323–351. 10.1080/00107510500052444

Numan, T., Breedt, L. C., Maciel, B. de A. P. C., Kulik, S. D., Derks, J., Schoonheim, M. M., . . . Douw, L. (2022). Regional healthy brain activity, glioma occurrence and symptomatology. *Brain*, *145*(10), 3654–3665. 10.1093/brain/awac180

O'Byrne, J., & Jerbi, K. (2022). How critical is brain criticality? *Trends in Neurosciences*, *45*(11), 820–837. 10.1016/j.tins.2022.08.007

Priesemann, V., & Shriki, O. (2018). Can a time varying external drive give rise to apparent criticality in neural systems? *PLOS Computational Biology*, *14*(5), e1006081. 10.1371/journal.pcbi.1006081

Pritchard, W. S. (1992). The brain in fractal time: 1/f-like power spectrum scaling of the human electroencephalogram. *International Journal of Neuroscience*, *66*(1–2), 119–129. 10.3109/00207459208999796

Pu, S., & Thomas, P. J. (2020). Fast and accurate Langevin simulations of stochastic Hodgkin-Huxley dynamics. *Neural Computation*, *32*(10), 1775–1835. 10.1162/neco_a_01312

Pu, S., & Thomas, P. J. (2021). Resolving molecular contributions of ion channel noise to interspike interval variability through stochastic shielding. *Biological Cybernetics*, *115*(3), 267–302. 10.1007/s00422-021-00877-7

Racz, F. S., Farkas, K., Stylianou, O., Kaposzta, Z., Czoch, A., Mukli, P., . . . Eke, A. (2021). Separating scale-free and oscillatory components of neural activity in schizophrenia. *Brain and Behavior*, *11*(5), e02047. 10.1002/brb3.2047

Robertson, M. M., Furlong, S., Voytek, B., Donoghue, T., Boettiger, C. A., & Sheridan, M. A. (2019). EEG power spectral slope differs by ADHD status and stimulant medication exposure in early childhood. *Journal of Neurophysiology*, *122*(6), 2427–2437. 10.1152/jn.00388.2019

Rudolph, M., Pelletier, J. G., Paré, D., & Destexhe, A. (2005). Characterization of synaptic conductances and integrative properties during electrically induced EEG-activated states in neocortical neurons in vivo. *Journal of Neurophysiology*, *94*(4), 2805–2821. 10.1152/jn.01313.2004

Schaworonkow, N., & Voytek, B. (2021). Longitudinal changes in aperiodic and periodic activity in electrophysiological recordings in the first seven months of life. *Developmental Cognitive Neuroscience*, *47*, 100895. 10.1016/j.dcn.2020.100895

Spyropoulos, G., Dowdall, J. R., Schölvinck, M. L., Bosman, C. A., Lima, B., Peter, A., . . . Fries, P. (2020). *Spontaneous variability in gamma dynamics described by a linear harmonic oscillator driven by noise*. bioRxiv, 793729. 10.1101/793729

Steyn-Ross, D., Steyn-Ross, M., Sleigh, J., Wilson, M., Gillies, I., & Wright, J. (2005). The sleep cycle modelled as a cortical phase transition. *Journal of Biological Physics*, *31*(3), 547–569. 10.1007/s10867-005-1285-2

Steyn-Ross, M. L., Steyn-Ross, D. A., & Sleigh, J. W. (2012). Gap junctions modulate seizures in a mean-field model of general anesthesia for the cortex. *Cognitive Neurodynamics*, *6*(3), 215–225. 10.1007/s11571-012-9194-0

Steyn-Ross, M. L., Steyn-Ross, D. A., Sleigh, J. W., & Liley, D. T. J. (1999). Theoretical electroencephalogram stationary spectrum for a white-noise-driven cortex: Evidence for a general anesthetic-induced phase transition. *Physical Review E*, *60*(6), 7299–7311. 10.1103/PhysRevE.60.7299

Steyn-Ross, M. L., Steyn-Ross, D. A., Sleigh, J. W., & Whiting, D. R. (2003). Theoretical predictions for spatial covariance of the electroencephalographic signal during the anesthetic-induced phase transition: Increased correlation length and emergence of spatial self-organization. *Physical Review E*, *68*(2), 021902. 10.1103/PhysRevE.68.021902

Steyn-Ross, M. L., Steyn-Ross, D. A., Sleigh, J. W., Wilson, M. T., & Wilcocks, L. C. (2005). Proposed mechanism for learning and memory erasure in a white-noise-driven sleeping cortex. *Physical Review E (Statistical, Nonlinear, and Soft Matter Physics)*, *72*(6 Pt. 1), 061910.

Strang, A. G., Abbott, K. C., & Thomas, P. J. (2019). How to avoid an extinction time paradox. *Theoretical Ecology*, *12*(4), 467–487. 10.1007/s12080-019-0416-5

Stumpf, M. P. H., & Porter, M. A. (2012). Critical truths about power laws. *Science*, *335*(6069), 665–666. 10.1126/science.1216142

Thomas, P. J., & Lindner, B. (2019). Phase descriptions of a multidimensional Ornstein-Uhlenbeck process. *Physical Review E*, *99*(6), 062221. 10.1103/PhysRevE.99.062221

Touboul, J., & Destexhe, A. (2010). Can power-law scaling and neuronal avalanches arise from stochastic dynamics? *PLOS One*, *5*(2), e8982. 10.1371/journal.pone.0008982

Traub, R. D., Buhl, E. H., Gloveli, T., & Whittington, M. A. (2003). Fast rhythmic bursting can be induced in layer 2/3 cortical neurons by enhancing persistent Na+ conductance or by blocking BK channels. *Journal of Neurophysiology*, *89*(2), 909–921. 10.1152/jn.00573.2002

Uhlhaas, P. J., & Singer, W. (2012). Neuronal dynamics and neuropsychiatric disorders: Toward a translational paradigm for dysfunctional large-scale networks. *Neuron*, *75*(6), 963–980. 10.1016/j.neuron.2012.09.004

Voytek, B., Kramer, M. A., Case, J., Lepage, K. Q., Tempesta, Z. R., Knight, R. T., & Gazzaley, A. (2015). Age-related changes in 1/f neural electrophysiological noise. *Journal of Neuroscience*, *35*(38), 13257–13265. 10.1523/JNEUROSCI.2332-14.2015

Wen, H., & Liu, Z. (2016). Separating fractal and oscillatory components in the power spectrum of neurophysiological signal. *Brain Topography*, *29*(1), 13–26. 10.1007/s10548-015-0448-0

Whittington, M., Traub, R., Kopell, N., Ermentrout, B., & Buhl, E. (2000). Inhibition-based rhythms: Experimental and mathematical observations on network dynamics. *International Journal of Psychophysiology*, *38*(3), 315–336. 10.1016/S0167-8760(00)00173-2

Wilson, H. R., & Cowan, J. D. (1972). Excitatory and inhibitory interactions in localized populations of model neurons. *Biophysical Journal*, *12*(1), 1–24. 10.1016/S0006-3495(72)86068-5

Wilson, L. E., da Silva Castanheira, J., & Baillet, S. (2022). Time-resolved parameterization of aperiodic and periodic brain activity. *eLife*, *11*, e77348. 10.7554/eLife.77348

Wilson, M. T., Sleigh, J. W., Steyn-Ross, D. A., & Steyn-Ross, M. L. (2006). General anesthetic–induced seizures can be explained by a mean-field model of cortical dynamics. *Anesthesiology*, *104*(3), 588–593. 10.1097/00000542-200603000-00026

Wilson, M. T., Steyn-Ross, D. A., Sleigh, J. W., Steyn-Ross, M. L., Wilcocks, L. C., & Gillies, I. P. (2006). The K-complex and slow oscillation in terms of a mean-field cortical model. *Journal of Computational Neuroscience*, *21*(3), 243–257. 10.1007/s10827-006-7948-6

Received November 7, 2023; accepted March 25, 2024.